Toward Intelligent Sensing: Optimizing LiDAR Beam Distribution for Autonomous Driving

Genghang Zhuang, Zhenshan Bing, Xiangtong Yao, Yuhong Huang, Kai Huang*, and Alois Knoll

***Abstract*—LiDAR (Light Detection And Ranging) sensors have been widely used in autonomous vehicles as the main sensors. According to the specification details of the widely used 3D LiDAR products in the market, the distribution of vertical beam channels is set according to a uniform angular resolution, which is not ideally efficient for specific autonomous tasks. In this paper, we propose a novel approach to find the optimized angular distribution of the vertical beam channels for different application scenarios and installation configurations. The experimental results in a study case suggest that concerning the vehicle detection task, the optimized LiDARs perform almost two times better than the ones with the same number of channels in terms of the detection range, and have perception performances close to the LiDARs with double channels in the long distance.**

***Index Terms*—LiDAR sensor, LiDAR optimization, autonomous driving.**

I. Introduction

THERE has been increasing interest in development of autonomous driving vehicles. In most applications, an autonomous vehicle requires a precise perception of the surrounding environment. Various sensors including LiDAR, radar, monocular camera, and stereo camera are successfully deployed in autonomous vehicles to implement perceiving tasks such as object detection and classification, as well as tracking. Among aforementioned sensors, LiDAR has been widely used in autonomous vehicles as the main sensor. In particular, 3D LiDAR sensors with multiple beam channels in vertical direction can accurately represent the surroundings as a 3D point cloud model by constantly scanning in 360°. Compared with cameras, LiDAR has an ability to directly obtain the depth information about objects in the environment without the necessity to be concerned about changes in illumination. There are numerous research works attempting to resolve the tasks on SLAM (Simultaneously Localization And Mapping) [1]–[3], global localization [4]–[6], lane detection [7], 3D objection detection [8] and segmentation [9] based on LiDAR sensors.

Currently, 3D LiDARs with multiple beam channels are still expensive, which in a way prevents the mass production deployment of autonomous vehicles. Concerning different scenarios, additional beam channels can provide higher angular resolution in the vertical direction. More importantly, it can be also helpful to collect more surface details of objects. However, the price of a 3D LiDAR is also proportional to the number of internal beam channels. Therefore, it is necessary and important to maximize the efficiency of limited channels.

Genghang Zhuang, Zhenshan Bing, Xiangtong Yao, Yuhong Huang, and Alois Knoll are with Department of Informatics, Technical University of Munich, Gemerny (Email: zhuang@in.tum.de; bing@in.tum.de; xiangtong.yao@tum.de; yuhong.huang@tum.de; knoll@in.tum.de).

Kai Huang*(corresponding author) is with School of Computer Science and Engineering; Shenzhen Institute, Sun Yat-sen University, China (Email: huangk36@mail.sysu.edu.cn).

According to the specification details of widely used 3D LiDAR products in the market, the distribution of vertical beam channels is defined as uniform angular resolution in the vertical range. In the most specific scenarios, the uniform angular resolution is not ideally efficient for autonomous vehicles for the two reasons. First, in the case of different perception objectives including pedestrians, vehicles, and obstacles, uniform angular resolution does not meet appropriately their specific requirements, such as for example, the height range of interest. Second, the uniform vertical resolution and fixed angular range are inappropriate for diverse installation configurations, such as the front, roof, and rear one of the vehicles for different scenarios and intentions. Although several most-recent LiDAR products introduce the nonlinear vertical angular distribution, the proprietary distribution pattern and setting basis remain unknown and are not available for public. Therefore, it is meaningful to propose an optimization algorithm and procedure for the beam channel distribution of LiDARs.

In this paper, we propose a concept and a corresponding approach to find the optimized angular distribution of the vertical beam channels intended for different application scenarios and installation configurations. The main idea of the proposed approach is to formulate the distribution problem of vertical channels as a weighted multi-objective optimization targeted to the essential features of autonomous driving perception. In the conducted experiments, as a proof-of-concept, a virtual LiDAR with flexible channels is implemented in the autonomous driving simulator CARLA [10], to evaluate the performance in terms of perception tasks of autonomous driving. The experimental results in simulator indicate that concerning the specific object detection task, the optimized LiDARs perform almost two times better than the ones with the same number of channels in terms of the detection range, and have the performance close to that of LiDARs with double channels with regard to the perception tasks in the long distance. The main contributions of the present work are as follows:

1) We optimize the angular distribution of vertical beam channels by formulating it into a multi-objective optimization problem, considering various requirements.
2) As a proof of concept, a flexible LiDAR module is developed in the CARLA simulator to customize the beam channel distribution and generate annotated points with the type information.
3) Evaluations on object detection and semantic segmentation considering different numbers of beam channels are proposed and conducted to demonstrate and evaluate the efficiency of the proposed approach. The results show the superior performance of the optimized LiDARs for multi-class object detection and lane segmentation.

Model	Channels	Vertical Field of View
Velodyne VLP-16	16	+15.0°to -15.0°(30.0°)
Velodyne HDL-32E	32	+10.67°to -30.67°(41.33°)
Velodyne HDL-64E	64	+2.0°to -24.9°(26.9°)

TABLE I
VIEW FIELD SPECIFICATIONS OF COMMON LIDAR PRODUCTS

II. RELATED WORK & BACKGROUND

In the related literature, there is rare research works focused on optimization of channel beam distribution of 3D LIDAR for the purpose of autonomous driving, and either the framework and general evaluation procedure of this channel optimizing problem. Many existing similar studies were dedicated to identifying the optimal placement configuration for multi-sensors. Dybedal et al. in [11] proposed an approach to resolve the problem of the optimal placement of 3D camera sensors in a specified volume of interest, where the coverage area of the sensors is modeled as a cone having the limited field of view and range. Mou et al. described an optimal LIDAR configuration approach in [12] proposed for autonomous cars, in which ROI (Region Of Interest) is segmented into the sub-spaces bounded by the surfaces of cones. However, the models and frameworks in aforementioned work are inapplicable for channel distribution optimization of a 3D LIDAR.

To evaluate the optimization of the proposed approach, we implement a virtual LIDAR and conduct the experiments in a high-fidelity simulator. The feasibility of evaluation in simulators is elaborated and demonstrated in several researches. An open-source driving simulator CARLA was detailed by Dosovitskiy et al. in [10]. Shah et al. from *Microsoft Research* described the *Airsim* simulator in [13], which provides a high-fidelity visual and physical simulation for autonomous vehicles. Most simulators for autonomous driving provide various urban scenarios and virtual sensors including camera, depth camera and 3D LIDAR. Researches in [14] [15] [16] attempted to utilize the sensor data obtained from autonomous driving simulators to generate the extensive annotated data for training and testing the neural networks of autonomous driving tasks. Compared with real LIDARS, virtual 3D LIDARS can directly obtain point clouds with collision detection in the physics engine. Experimental results provided in [17] demonstrated the high fidelity of virtual LIDAR. Therefore, it is feasible to evaluate virtual 3D LIDARS in autonomous driving simulators.

III. MOTIVATION

In general, common 3D LIDAR products share the same rotation structure. LIDAR rotates in the horizontal plane. With the embedded rotation encoder and high-frequency beam ejector, LIDAR can achieve high horizontal resolution. However, the vertical resolution of a LIDAR only depends on the multiple beam channels. Limited by the cost of beam ejectors, the vertical resolution of common LIDAR products is much lower than the horizontal resolution.

TABLE I provides specifications of the vertical view field of the common LIDAR products. The vertical channels of the listed 3D LIDAR products are distributed evenly in the range. For autonomous driving tasks, 3D LIDAR have to provide a sufficient number of surface points on objects. To quantize the influence of the channel distribution on the valid casted points, we model the listed common 3D LIDAR products and compute the number of valid points, which are casted on the surface of the target object, in different conditions.

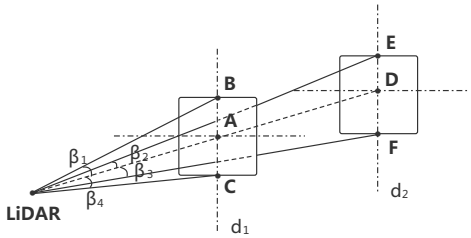

(a) Sketch of LIDAR beams

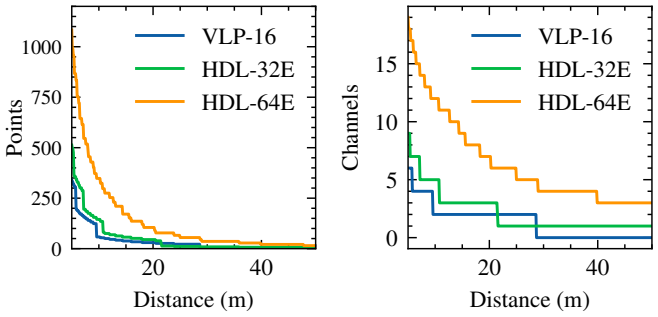

(b) Points (c) Beam channels

Fig. 1. Points and beam channels on $1m^2$ object for different distances.

Fig. 1a illustrates the beam casting on a $1\,m^2$ object in distance d_1 and d_2, in which the beams of small angles β_2 and β_3 are able to cast on a further object. Fig. 1b and Fig. 1c represent the numbers of casting points and beams on a $1\,m^2$ object for the three different 3D LIDARS with different distances. Caused by the decline in the casted vertical beams on the object with distance, the number of casted points decreases considerably over 20 m. The provided figures indicate the low density of casted points in long distances, which may affect the precision of object detection and classification. Therefore, to use efficiently each beam of a 3D LIDAR, we propose an algorithm to determine the optimized angular distribution of the vertical beam channels.

IV. LIDAR FORMULATION

To investigate the influence of the angular distribution of the vertical beam channels on the performance of the specific perception tasks, we model and implement a virtual LIDAR on the CARLA platform. The virtual LIDAR is optimized accordingly, as detailed in SECTION V.

A. Rotation Model

The LIDAR rotates in the horizontal plane to obtain a 360°view of the horizontal field. The LIDAR scans at the same interval and produces a sequence of endpoints. The values of horizontal ranging angles can be defined as follows:

$$rotation = \left\{\theta_i, i = 0, 1, ..., m\right\}, \tag{1}$$

where the number of horizontal ranging steps m is determined by the horizontal resolution, $m = {}^{2\pi}/_{resolution}$.

Because of the restriction of the mechanical structure and scanning efficiency, the common 3D LIDARS do not contain the rotating structure in the vertical plane. Instead, a fixed number of multiple beam ejectors are equipped in LIDAR, as

shown in Fig. 1a. The angular distribution of the vertical beam channels can be defined as the following vector:

$$\mathbf{c} = \Big(\ \beta_1, \ \beta_2, \ \ldots, \ \beta_j \Big)^T \ , \tag{2}$$

where the j is the number of vertical channels and β is negative when the beam is heading down. Here, $\mathbf{c}$ is the variable to be optimized in this work.

B. Installation Configuration

Autonomous vehicle platforms generally are equipped with 3D LiDARs in various positions for different perception targets. For example, most of autonomous vehicles utilize a 3D LiDAR on the roof to perform object detection in the medium distance. In other particular cases, an additional LiDAR can be installed at the front of the vehicle to detect small objects near to the vehicle. Therefore, the angular distribution of vertical channels should consider different intended usages and installation configuration.

In distribution optimization and evaluation, the installation height h and the heading angle φ in the horizontal plane of LiDAR are considered. During the process of optimization, h is an important influence factor to be considered and h and φ are required for pre-processing, which are applied to transform a point cloud into the reference frame of vehicle for further object detection.

V. Optimization

To optimize the channel distribution $\mathbf{c}$, we formulate it as a multi-objective optimization problem as follows:

$$\begin{aligned} \mathcal{F}(\mathbf{c}) &= \sum_k \gamma_k \cdot \mathcal{F}_k(\mathbf{c}) \\ \mathbf{c}^* &= \underset{\mathbf{c}}{\operatorname{argmax}} \sum_k \gamma_k \cdot \mathcal{F}_k(\mathbf{c}) \ , \end{aligned} \tag{3}$$

where the $\mathcal{F}(\mathbf{c})$ consisting of weighted sub-objectives is the overall objective function and $\mathbf{c}^*$ denotes the optimized channel distribution when $\mathcal{F}(\mathbf{c})$ is maximized. The sub-objective is defined as $\mathcal{F}_k(\mathbf{c})$ and its corresponding coefficient is denoted as γ_k. The sub-objective in (3) contributes to the overall objective in terms of different aspects. Their corresponding sub-problems include the channel dispersal in the short distance, focusing on the medium and long distances, and blind zone avoidance in the installation area.

A. Distribution Dispersal for Channels

LiDAR should be able to detect and track objects close to the autonomous vehicle, including pedestrians, vehicles, and obstacles. To obtain a wide view in the vertical direction, the channels should be dispersed within an appropriately decent range. The objective function of dispersal capacity is formulated as follows:

$$\mathcal{F}_{dis}(\mathbf{c}) = \int \delta_{dis}(\mu) \cdot Dis(\mu, \mathbf{c}, h) \, \mathrm{d}\mu, \mu \in ROI \ , \tag{4}$$

where the sub-objective function $\mathcal{F}_{dis}(\mathbf{c})$ evaluates the dispersal of $\mathbf{c}$ over the range of distances μ in a pre-specified ROI (Region Of Interest). The dispersal in a certain distance is based on the evaluation value $Dis(\mu, \mathbf{c}, h)$ and its corresponding weight coefficient $\delta_{dis}(\mu)$. The weight coefficient function is defined with the distances of interest as follows:

$$\delta(\mu) = -\prod_i \left(\frac{\mu - \mu_{interest\_i}}{s_i}\right)^2 + 1 \ , \tag{5}$$

where $\mu_{interest\_i}$ is the i-th distance of interest and s_i is the corresponding scaling value. The coefficient function is used to focus the dispersal in a particular range of the distances of interest, and $\delta(\mu)$ reaches the maximum in the distance $\mu_{interest\_i}$. $Dis(\mu, \mathbf{c}, h)$ in (4) corresponds to dispersal evaluation on channels distribution $\mathbf{c}$ in distance μ:

$$Dis(\mu, \mathbf{c}, h) = Range(I(\mu, \mathbf{c}, h)) \ , \tag{6}$$

where $I(\mu, \mathbf{c}, h)$ is a filter defined to eliminate the channels in which beams impact on the ground surface at distance μ as follows:

$$I(\mu, \mathbf{c}, h) = \Big(\beta_i \cdot step(h + \mu \cdot tan\, \beta_i), i = 0, 1, ..., j\Big)^T, \tag{7}$$

where each angle β of beam in distribution $\mathbf{c}$ is filtered with the step function, in which the filtering is determined by the casted height at the vertical plane at distance μ. In (6), to describe the dispersal at μ, $Range(I(\mu, \mathbf{c}, h))$, the range of values of elements in $I(\mu, \mathbf{c}, h)$, indicating the impacting beams on the vertical plane at μ, is taken into account. Subsequently, the value is scaled in optimization implementation.

B. Distribution Focusing for Channels

In medium and long distances, it is difficult to maintain high precision of detecting or tracking objects due to the low resolution in the vertical direction. Therefore, the distribution of vertical channels should focus on the medium and long distances to achieve better scanning of objects.

For the focusing optimization, a sub-objective is constructed to evaluate channel focusing as follows:

$$\mathcal{F}_{foc}(\mathbf{c}) = \int \delta_{foc}(\mu) \cdot Foc(\mu, \mathbf{c}, h) \, \mathrm{d}\mu, \mu \in ROI \ , \tag{8}$$

where the $\delta_{foc}(\mu)$ defined in (5) is the corresponding coefficient function for the focusing problem. In (8), to evaluate focusing, the $Foc(\mu, \mathbf{c}, h)$ is computed and accumulated for the distribution $\mathbf{c}$ over the ROI as follows:

$$Foc(\mu, \mathbf{c}, h) = Count(I(\mu, \mathbf{c}, h)) \ , \tag{9}$$

where the $Count(\mu, \mathbf{c}, h)$ counts the non-zero values of casted beams in $I(\mu, \mathbf{c}, h)$ on the vertical plane in distance μ, and the values are further accumulated for optimization.

C. Blind Zone Avoiding Constraint

In several installation configurations, the vertical view field of 3D LiDAR will be reduced because of the blind zones. For example, LiDAR installed on the roof of the vehicle is the most common installing configuration for autonomous driving vehicle platforms. In such case, several channel beams of the large pitch angle may have impact on the roof surface, which will constantly produce a large number of indifferent points. Consequently, the distribution of channels $\mathbf{c}$ should assure that the beams do not cast on the blind zone. This can be achieved with the following constraint:

$$\mathcal{F}_{blind}(\mathbf{c}) = \int Blind(\mu, \mathbf{c}, h) \, \mathrm{d}\mu, \mu \in BZ. \tag{10}$$

The objective accumulates the cost to constrain the violation, where $Blind(\mu, \mathbf{c}, h)$ is the penalty cost defined as follows:

$$Blind(\mu, \mathbf{c}, h) = -\Big(\frac{j - Count\big(I(\mu, \mathbf{c}, h)\big)}{s}\Big)^n \ . \tag{11}$$

$Blind(\mu, \mathbf{c}, h)$ is based on the polynomial approximation of the constraint to beams impacting on horizontal plane inside

the blind zone; here, j is the number of channels in (2), and s denotes the corresponding scaling value and n is for the polynomial order for approximation.

D. Optimization Implementation

In the present work, optimization for the angular distribution of the vertical beam channels is implemented through a two-stage framework. Because of the multiple dimension of the channel $\mathbf{c}$, optimization can be highly computationally consuming. To reduce the overall complexity, coarse optimization is proposed to obtain a coarse result of the optimized channel distribution. The optimization result in coarse stage is refined in the next stage.

In the implementation, the objective defined in (3) is firstly transformed to the least squares problem as follows:

$$\begin{aligned}\mathbf{c}^* &= \underset{\mathbf{c}}{\operatorname{argmax}} \sum_k \gamma_k \cdot \mathcal{F}_k(\mathbf{c}) \\ &= \underset{\mathbf{c}}{\operatorname{argmin}} \sum_k \left(\gamma_k \cdot \sum_\mu \left(1 - sigmoid(\mathcal{F}_k(\mathbf{c}, \mu))\right)^2\right),\end{aligned} \tag{12}$$

where the values of sub-objective $\mathcal{F}_k(\mathbf{c})$ for distances μ are scaled to $(0, 1)$ and inverted. Therefore, in such way, the problem can be transformed into a nonlinear optimization problem. In coarse optimization process, a candidate set of channel distributions is generated with a specified resolution, upper bound, and lower bound of the range. All the distributions in the candidate set are enumerated, and the distribution with the highest objective evaluation is outputted as the initial estimate for the refinement. In the process of refinement, the coarsely optimized channel distribution is further refined. As a result, the optimized channel distribution $\mathbf{c}$ is obtained.

VI. Case Studies for Autonomous Driving Tasks

To evaluate the performance of the optimized LiDARs, we conduct the evaluation on object detection and semantic segmentation for the original and the optimized LiDARs relying on the proposed optimization. Firstly, an SVM-based efficient algorithm for vehicle detection is implemented and applied in the experiments to evaluate the performances of different LiDARs and reflect the influence of casting points over distances. Secondly, to further test the optimized LiDARs in common autonomous driving perception tasks, we utilize a convolutional neural network model (CNN) to perform object detection experiments on cars, cyclists, and pedestrians. Thirdly, we employ a semantic segmentation network to evaluate lane segmentation performances for optimized LiDARs.

A. Vehicle Detection Based on Handcrafted Features

In the first evaluation, we applied a method on the basis of the clustering and classification procedure for the vehicle detection task based on handcrafted features. In the process of clustering, the points on the ground plane are first excluded to eliminate the impact on the point cloud clustering for different objects. Subsequently, clustering based on the Euclidean distance is performed on the point cloud.

As the objects of the same type share a similar spatial distribution in the point cloud [18], it is efficient and feasible to utilize features so as to represent the distribution of points in order to distinguish the targets. When extracting features from clusters, a feature fusion including both local and global features is adopted. Local features reckoned with the neighborhood of points are utilized to describe the local spatial distribution. In this work, the *FPFH* (Fast Point Feature Histograms) histogram feature is used, which estimates the local spatial distribution with the relative angles between the normal vector and the connection vector in the neighborhoods of points [19]. Besides local features, global features based on *VFH* (viewpoint feature histogram) are extracted to describe the global distribution of the point cloud, in which the pose and surface histogram features are taken into account [20].

In the process of cluster classification, Support Vector Machine (*SVM*) classification exploiting the extracted features is implemented to detect the objective clusters, in which the object detection is conducted as a binary classification for the point cloud clusters.

B. DNN-Based Object Detection

In order to further evaluate the performance of the optimized LiDARs for generalized objection detection, we utilize the LiDAR-based Complex-YOLO [21] CNN model to perform detection for car, cyclist, and pedestrian. Complex-YOLO is a widely used and implemented deep neural network targeted for 3D object detection with LiDAR sensor. The model was trained and tested on the KITTI dataset [22] and showed its high performance and efficiency in detecting cars, cyclists, and pedestrians in the range of $40\,\mathrm{m}$. In the evaluation, we exploit the pre-trained model, which is trained and targeted for *Velodyne HDL-64E*, to test and compare the performances of optimized and original 16- and 32-channel LiDARs. To avoid the potential overfitting issue and considering that the model is already well generalized to various scenarios, the neural model would not be re-trained to adapt LiDARs with different numbers of channels in the evaluation. The original *HDL-64E* is also evaluated to provide a baseline for other LiDARs.

C. DNN-Based Semantic Segmentation for Lane Area

Besides object detection, semantic segmentation is also a common perception task for autonomous vehicles. In order to further reflect the performance differences over distance, we carry out the drivable lane area segmentation in this part of evaluation. A fully convolutional neural network (FCN) [7], [23] is implemented in this work to perform lane segmentation based on LiDAR point cloud. Similarly, the model is trained with the point cloud data from *HDL-64E* and utilized to evaluate the optimized and original 16- and 32-channel LiDARs.

VII. Evaluation Results

Experiments on original and optimized LiDARs are conducted to investigate the performance in the scenario of autonomous driving. To provide a proof-of-concept, test and evaluate the proposed approach, we design and implement the virtual LiDAR and conduct the experiments in the CARLA [10] simulator. In the experiments, we study the case of perception with one LiDAR placed on the roof of the vehicle, which is a common setting in the scenarios of autonomous driving, with the $h = 2.0, \varphi = 0$. The ROI and blind zone in the experiments are set as follows: $ROI = [5.0, 50.0], BZ = [0, 4.3]$. The domain of β is limited to be negative because of the installation height $h = 2.0$. Concerning the dispersal objective, we adopt $\gamma_{dis} = 1.0$, and then we set a typical distance of interest $\mu_{dis\_1} = 5.0$ in $\delta_{dis}(\mu)$ and its scaling $s_{dis\_1} = 20.0$. For the

Model	Beam Angles
Optimized-16	0.00, −1.00, −2.00, −2.27, −2.54, −2.86, −5.71, −7.00, −7.59, −9.00, −10.00, −11.00, −11.30, −13.00, −14.00, −21.80
Optimized-32	0.00, −0.50, −1.0, −1.50, −1.70, −1.86, −2.27, −2.34, −2.41, −2.54, −2.75, −3.00, −3.81, −5.71, −7.00, −7.29, −7.40, −7.50, −9.00, −9.24, −9.50, −10.00, −10.50, −11.00, −11.15, −11.30, −13.00, −13.50, −14.00, −15.95, −17.90, −21.80

TABLE II
OPTIMIZED LIDAR BEAM DISTRIBUTION

focusing objective, we adopt $\gamma_{con}=5.0$, a typical distance of interest $\mu_{con\_1}=50.0$ in $\delta_{foc}(\mu)$, and its scaling $s_{con\_1}=20.0$.

A. Experimental Setup

The virtual LIDAR module in CARLA does not allow irregular channel distribution. For experimental purposes, we developed a new configurable LIDAR module in which the channel distribution can be customized for given parameters. We can also directly obtain the semantic labels for the point cloud from the LIDAR. In the experiments, various actor agents were placed 5m ahead the autonomous vehicle, and were driven out of the scan range of LIDAR to test the perception capacity described in SECTION VI. The scenario is set so as to evaluate the detection performance of the optimized LIDAR from the short distance to the medium and long distances. We evaluate the five settings of LIDAR with the uniform distribution of 16, 32, and 64 channels in specifications of *Velodyne*, and the optimized distribution of 16 and 32 channels.

We first list the angle values of the optimized LIDARs in TABLE II. In the distribution of the optimized 16-channel and 32-channel LIDAR, the overall density of beams increases as the distribution range shifts from [-15.0, 15.0] and [-30.67, 10.67] to [-21.80, 0]. Beams are dispersed in $\mu_{dis\_1}=5.0$ according to the typical distance of interest of dispersal set in advance, which enables the LIDAR to obtain much more details for the close objects. In addition, the beams are still focused on the further distance due to the $\mu_{con\_1}=50.0$ typical distance of interest corresponding to the beam focusing in optimization. This adjustment increases the potential of LIDAR to detect objects in the long distance. The result demonstrates the ability of the proposed approach to optimize the dispersal and focusing for LIDAR beams with given settings.

B. SVM-Based Vehicle Detection

In the experiments on the vehicle detection, we report the results for the detection range, as represented in Fig. 2. The diagram illustrates the distance range and the median distance

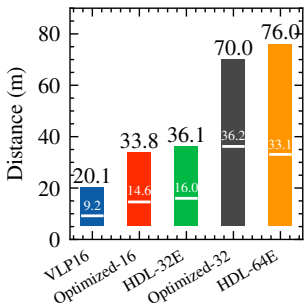

Fig. 2. Vehicle detection range

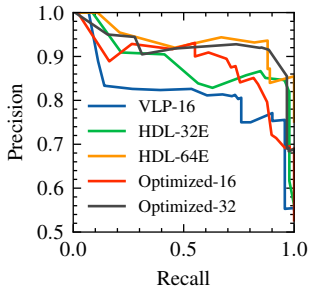

Fig. 3. Precision-recall curves

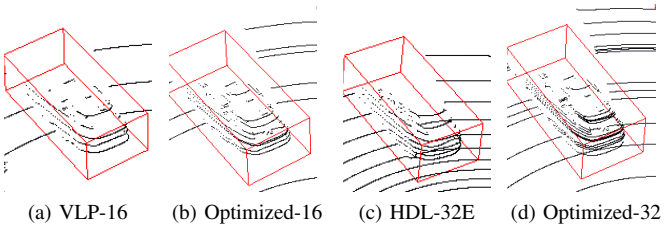

Fig. 4. Point clouds on vehicle of different LIDARs in a medium distance

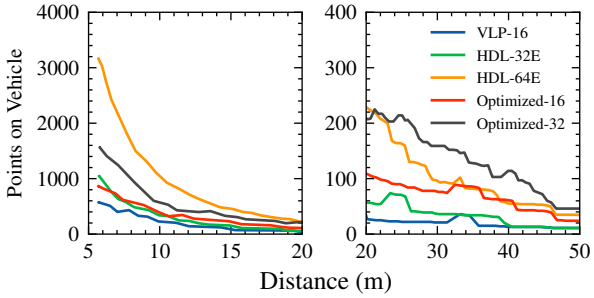

Fig. 5. Points on target vehicle over distances (the higher, the better)

of true positive cases of detecting the target vehicles starting from 5m. The top of the boxes indicate the upper bounds of the detection ranges. The figure shows that the distribution obtained by the proposed approach outperforms the uniform distribution for both 16-channel and 32-channel settings. There are obvious increases in the range for optimized 16-channel and 32-channel LIDAR. Given the same number of channels, the longest detectable distances increase up to 68.0% and 93.9% for 16 and 32 channels, respectively. For the optimized-32 setting, the longest distance is close to that of *HDL-64E*. We also report the precision and recall in Fig. 3. The closer the curve to the upper-right corner the better is the result. The figure represents the precision-recall curves of vehicle detection in the medium distance range (15m - 30m). The clear trend indicates that the optimized LIDARs have higher precision and recall compared with the original ones. For the same recall rate, the precision of the optimized LIDARs increases up to 13.9% for 16-channel and up to 12.1% for 32-channel. For certain cases, the Optimized-16 LIDAR outperforms *HDL-32E*, and Optimized-32 is even better than *HDL-64E*.

To perform object detection in different distances for the target vehicle, LIDARs require the sufficient number of points casted on the object. Fig. 4 shows the points casted on a vehicle of different LIDARs in a medium distance. As shown in the figures, the points casted by the optimized LIDARs are denser compared with those of the original ones. Fig. 5 outlines the number of points casted on the vehicle with different distances. LIDARs with more channels have higher vertical resolution and produce more points on the target vehicle in the long distances, as discussed in Fig. 1. In the distance range from $5m$ to $20m$, the obtained numbers of points in aggregate for the optimized LIDARs increase 72.2% and 88.5% of that for 16 and 32 channels, respectively. For the range from $5m$ to $50m$, the numbers increase 102.2% and 129.5%. In addition, the number for the optimized 16 channels is 16.6% better for the range from $5m$ to $20m$, and 34.2%

LiDAR	Car		Cyclist		Pedestrian	
	5-20m	20-40m	5-20m	20-40m	5-20m	20-40m
HDL-64E	89.66	81.87	73.27	58.62	51.01	43.15
Optimized-32	85.40	67.93	61.86	35.21	39.70	35.34
HDL-32E	63.80	35.92	49.38	28.05	35.77	1.4
Optimized-16	44.93	29.22	43.60	3.06	37.31	/
VLP-16	29.57	18.93	27.39	/	29.15	/

TABLE III
AP (%) COMPARISON FOR DNN-BASED OBJECT DETECTION

LiDAR	Pixel Accuracy (%)		IoU (%)	
	2-20m	20-50m	2-20 m	20-50m
HDL-64E	99.03	98.34	95.33	89.74
Optimized-32	98.19	98.37	91.49	89.50
HDL-32E	98.06	97.93	90.83	87.07
Optimized-16	97.25	90.00	86.99	42.23
VLP-16	95.11	85.84	77.60	13.59

TABLE IV
PERFORMANCE COMPARISON FOR DNN-BASED LANE SEGMENTATION

better for $5m$ to $50m$ than that of *HDL-32E*.

C. CNN-based Object Detection

In TABLE III we present the object detection results based on the Complex-YOLO network for three object types grouped by different distance ranges. Average Precision (AP) results are computed to show the average detection performance for different LiDARs. The DNN model is pre-trained with the KITTI dataset which is based on a *Velodyne HDL-64E* LiDAR. Therefore, in this testing setup, the original *HDL-64E* LiDAR as a baseline shows the highest performance among the evaluated LiDARs. The results show that the optimized LiDARs generally perform better than the original LiDARs in medium and long distances, due to the concentrated channel distribution. The performance of optimized-32 LiDAR is close to *HDL-64E* in car detection, and optimized-16 LiDAR performs close to *HDL-32E* in cyclist and pedestrian detection. Both optimized and original 16-channel LiDARs barely recognize cyclists and pedestrians in 20-40m, and there are also very few positive cases of pedestrian detection in 20-40m for *HDL-32E*. Considering the model is trained with the KITTI dataset based on the 64-channel LiDAR for urban scenes, we presume the network is trained to tolerate noise and therefore needs denser point clouds on small objects to distinguish the targets.

D. Semantic Segmentation for Lane Area

TABLE IV shows the performance comparison in the lane segmentation task. Pixel accuracy and Intersection Over Union (IoU) are evaluated for different ranges of distance, which are the most common metrics for semantic segmentation. The pixel accuracy results are relatively high because the lane area is small within the scene, which biases the measure to negative cases to some degree. As shown in the table, optimized 16 and 32-channel LiDARs outperform the original LiDARs in both 2-20m and 20-50m distance ranges on pixel accuracy and IoU. Optimized-32 LiDAR has a close performance to the baseline in 20-50m. Optimized-16 LiDAR outperforms the original 16-channel LiDAR by 2 times regarding IoU in 20-50m distance.

VIII. DISCUSSION

Because of the limitation of the current LiDAR products, at present, it is still not practical to customize and implement the optimized LiDAR products after production. Therefore, we implemented a configurable LiDAR in the simulator for evaluation. In the experiments, to reduce the complexity of the overall procedure, deep neural networks whose architectures are heavily subject to the changes of input size for different LiDARs are not introduced in the present study. Instead, the pre-trained CNN-based and FCN-based networks, which can adapt to different vertical channels, are employed.

In optimization, although the two-stage optimizing procedure greatly reduces the computing complexity, the whole process is still time-consuming, especially, when the dimension of **c** increases. Therefore, in the present study, we focus on the optimization for LiDARs with low beam density, that is, the 16-channel and 32-channel LiDARs, which can better demonstrate the differences for the beam channel optimization. The results of the original 64-channel LiDAR are retained to provide a performance baseline for the optimized 32-channel LiDAR.

The proposed research can be helpful and intriguing for LiDAR designing and customization. For LiDARs with limited channels, the method can be applied to improve the perception performance by focusing the beams in the range corresponding to the objects of interest, effectively reducing the deployment costs of LiDAR by improving the perception efficiency over channels, while proper tuning can help ensure the necessary coverage for the short distance. There is also a potential for high-density LiDARs to benefit from channel optimization. By introducing a mechanism to selectively retain essential channels and shut down the temporarily indifferent ones for different scenarios, LiDAR will be able to actively save power and reduce information redundancy with less involved channels, which is especially beneficial for power-constrained vehicles. The flexibility can help vehicles in low power mode to further reduce power consumption and at the same time maintain necessary perception reliability. Although it is still a high cost to customize conventional LiDAR products in common cases, with the rapid development of solid-state LiDAR which can adjust the vertical distribution of beams easier [24], the proposed approach can be easily deployed and applied to potentially improve the overall performance, power efficiency, and scan latency. The beam adjustment for solid-state LiDARs can be in real-time and scenario-oriented, in which the scenario-specific configurations can be deployed dynamically. By now, there are rare detailed public specifications or data regarding non-linear channel distribution LiDAR, nor the research for the related optimization method and framework. We hope this work can potentially trigger other related research. In the future, we plan to conduct additional experiments regarding optimized LiDARs in comparison with other existing non-linear LiDAR products. In addition, we intend to conduct experiments on selective channels to investigate channel significance in regard to power consumption for high density LiDARs such as 64- and 128-channel LiDARs. Furthermore, we are proposing potential deployments and experiments on power-constrained embedded robot platforms, in a combination of other low power consumption approaches for autonomous navigation [25]–[28].

IX. Conclusion

In this paper, we propose an approach to find the optimized angular distribution of vertical beam channels for specific application scenarios. We conduct the evaluation of object detection and semantic segmentation for the optimized 3D LiDARs in the autonomous driving simulator. The experimental results suggest that concerning the specific object detection task, the optimized LiDARs perform almost two times better than the ones with the same number of channels in the detection range, and have a performance close to the LiDARs with double channels in the long distance. At last, the limitations and prospects of the present study are discussed.

Acknowledgment

This research was supported in part by the Shenzhen Basic Research Grants with No. JCYJ20180508152434975 & No. JCYJ20210324122203009, in part by the Science and Technology Planning Project of Guangzhou city of China with No. 202007050004 and in part by the National Natural Science Foundation of China with No. 62232008.

References

[1] J. Zhang and S. Singh, "Loam: Lidar odometry and mapping in real-time." in *Robotics: Science and Systems*, vol. 2, 2014, p. 9.

[2] W. Hess, D. Kohler, H. Rapp, and D. Andor, "Real-time loop closure in 2d lidar slam," in *2016 IEEE international conference on robotics and automation (ICRA)*. IEEE, 2016, pp. 1271–1278.

[3] G. Zhuang, Z. Bing, Y. Huang, K. Huang, and A. Knoll, "A biologically-inspired simultaneous localization and mapping system based on lidar sensor," in *2022 IEEE/RSJ International Conference on Intelligent Robots and Systems (IROS)*. IEEE, 2022, pp. 13 136–13 142.

[4] R. W. Wolcott and R. M. Eustice, "Fast lidar localization using multiresolution gaussian mixture maps," in *2015 IEEE international conference on robotics and automation (ICRA)*. IEEE, 2015, pp. 2814–2821.

[5] G. Wan, X. Yang, R. Cai, H. Li, Y. Zhou, H. Wang, and S. Song, "Robust and precise vehicle localization based on multi-sensor fusion in diverse city scenes," in *2018 IEEE international conference on robotics and automation (ICRA)*. IEEE, 2018, pp. 4670–4677.

[6] G. Zhuang, C. Cagnetta, Z. Bing, H. Cao, X. Li, K. Huang, and A. Knoll, "A biologically-inspired global localization system for mobile robots using lidar sensor," in *2022 IEEE Intelligent Vehicles Symposium (IV)*. IEEE, 2022, pp. 984–990.

[7] L. Caltagirone, S. Scheidegger, L. Svensson, and M. Wahde, "Fast lidar-based road detection using fully convolutional neural networks," in *2017 IEEE Intelligent Vehicles Symposium (IV)*. IEEE, 2017, pp. 1019–1024.

[8] B. Yang, W. Luo, and R. Urtasun, "Pixor: Real-time 3d object detection from point clouds," in *Proceedings of the IEEE Conference on Computer Vision and Pattern Recognition*, 2018, pp. 7652–7660.

[9] C. R. Qi, H. Su, K. Mo, and L. J. Guibas, "Pointnet: Deep learning on point sets for 3d classification and segmentation," in *Proceedings of the IEEE Conference on Computer Vision and Pattern Recognition*, 2017, pp. 652–660.

[10] A. Dosovitskiy, G. Ros, F. Codevilla, A. Lopez, and V. Koltun, "CARLA: An open urban driving simulator," in *Proceedings of the 1st Annual Conference on Robot Learning*, 2017, pp. 1–16.

[11] J. Dybedal and G. Hovland, "Optimal placement of 3d sensors considering range and field of view," in *2017 IEEE International Conference on Advanced Intelligent Mechatronics (AIM)*. IEEE, 2017, pp. 1588–1593.

[12] S. Mou, Y. Chang, W. Wang, and D. Zhao, "An optimal lidar configuration approach for self-driving cars," *arXiv preprint arXiv:1805.07843*, 2018.

[13] S. Shah, D. Dey, C. Lovett, and A. Kapoor, "Airsim: High-fidelity visual and physical simulation for autonomous vehicles," in *Field and service robotics*. Springer, 2018, pp. 621–635.

[14] M. Johnson-Roberson, C. Barto, R. Mehta, S. N. Sridhar, K. Rosaen, and R. Vasudevan, "Driving in the matrix: Can virtual worlds replace human-generated annotations for real world tasks?" *arXiv preprint arXiv:1610.01983*, 2016.

[15] M. Martinez, C. Sitawarin, K. Finch, L. Meincke, A. Yablonski, and A. Kornhauser, "Beyond grand theft auto v for training, testing and enhancing deep learning in self driving cars," *arXiv preprint arXiv:1712.01397*, 2017.

[16] B. Wu, A. Wan, X. Yue, and K. Keutzer, "Squeezeseg: Convolutional neural nets with recurrent crf for real-time road-object segmentation from 3d lidar point cloud," in *2018 IEEE International Conference on Robotics and Automation (ICRA)*. IEEE, 2018, pp. 1887–1893.

[17] X. Yue, B. Wu, S. A. Seshia, K. Keutzer, and A. L. Sangiovanni-Vincentelli, "A lidar point cloud generator: from a virtual world to autonomous driving," in *Proceedings of the 2018 ACM on International Conference on Multimedia Retrieval*. ACM, 2018, pp. 458–464.

[18] R. B. Rusu, N. Blodow, Z. C. Marton, and M. Beetz, "Aligning point cloud views using persistent feature histograms," in *2008 IEEE/RSJ International Conference on Intelligent Robots and Systems*. IEEE, 2008, pp. 3384–3391.

[19] R. B. Rusu, N. Blodow, and M. Beetz, "Fast point feature histograms (fpfh) for 3d registration," in *2009 IEEE International Conference on Robotics and Automation*. IEEE, 2009, pp. 3212–3217.

[20] R. B. Rusu, G. Bradski, R. Thibaux, and J. Hsu, "Fast 3d recognition and pose using the viewpoint feature histogram," in *2010 IEEE/RSJ International Conference on Intelligent Robots and Systems*. IEEE, 2010, pp. 2155–2162.

[21] M. Simony, S. Milzy, K. Amendey, and H.-M. Gross, "Complex-yolo: An euler-region-proposal for real-time 3d object detection on point clouds," in *Proceedings of the European Conference on Computer Vision (ECCV) Workshops*, 2018, pp. 0–0.

[22] A. Geiger, P. Lenz, and R. Urtasun, "Are we ready for autonomous driving? the kitti vision benchmark suite," in *Conference on Computer Vision and Pattern Recognition (CVPR)*, 2012.

[23] J. Long, E. Shelhamer, and T. Darrell, "Fully convolutional networks for semantic segmentation," in *Proceedings of the IEEE conference on computer vision and pattern recognition*, 2015, pp. 3431–3440.

[24] C. V. Poulton, A. Yaacobi, D. B. Cole, M. J. Byrd, M. Raval, D. Vermeulen, and M. R. Watts, "Coherent solid-state lidar with silicon photonic optical phased arrays," *Optics letters*, vol. 42, no. 20, pp. 4091–4094, 2017.

[25] Z. Bing, C. Meschede, K. Huang, G. Chen, F. Rohrbein, M. Akl, and A. Knoll, "End to end learning of spiking neural network based on r-stdp for a lane keeping vehicle," in *2018 IEEE international conference on robotics and automation (ICRA)*. IEEE, 2018, pp. 4725–4732.

[26] Z. Bing, C. Meschede, G. Chen, A. Knoll, and K. Huang, "Indirect and direct training of spiking neural networks for end-to-end control of a lane-keeping vehicle," *Neural Networks*, vol. 121, pp. 21–36, 2020.

[27] Z. Bing, A. E. Sewisy, G. Zhuang, F. Walter, F. O. Morin, K. Huang, and A. Knoll, "Toward cognitive navigation: Design and implementation of a biologically inspired head direction cell network," *IEEE Transactions on Neural Networks and Learning Systems*, vol. 33, no. 5, pp. 2147–2158, 2021.

[28] Z. Bing, D. Nitschke, G. Zhuang, K. Huang, and A. Knoll, "Towards cognitive navigation: A biologically inspired calibration mechanism for the head direction cell network," *Journal of Automation and Intelligence*, vol. 2, no. 1, pp. 31–41, 2023.